ELSEVIER

Journal of Physics and Chemistry of Solids 61 (2000) 75–85

JOURNAL OF PHYSICS AND CHEMISTRY OF SOLIDS

www.elsevier.nl/locate/jpcs

Sb-doping effects on optical and electrical parameters of SnO_2 films

E.Kh. Shokr*, M.M. Wakkad, H.A. Abd El-Ghanny, H.M. Ali

Physics Department, Faculty of Science, Sohag, Egypt

Received 8 December 1998; accepted 3 June 1999

Abstract

Undoped and Sb-doped SnO_2 films $\sim$ 100 nm thick have been deposited by electron beam evaporation from bulk samples prepared using sintering technique. Either undoped or Sb-doped SnO_2 films are nearly amorphous, resistive and transparent. With increasing Sb content, the resistivity slightly decreases and then increases with further addition of Sb, which acts as donor and/or acceptor impurity atom in the SnO_2 lattice, respectively. Besides, the doping of Sb inside the SnO_2 lattice was associated with the increase in the film transmission at solar maximum wavelength and the width of optical band gap; which were interpreted in terms of the interaction between the two oxidation states of antimony, Sb^{3+} and Sb^{5+} and the increase of atomic bond energy, respectively. Moreover, the addition of Sb to the SnO_2 lattice has proved to affect significantly on the refractive index, the extinction coefficient, concentration of free carriers, dielectric constant, electric carrier susceptibility and Mott's parameters, which have been explained and correlated to the film microstructure change. © 1999 Elsevier Science Ltd. All rights reserved.

Keywords: Sb–Sn–O films; D. Microstructure

1. Introduction

Because of the high transparency and low resistivity SnO_2-based thin films, combined with mechanical hardness and good environmental stability, they have found a wide range of application [1–6].

Undoped tin oxide films are semiconductors with a wide band gap [7–9] and tetragonal rutile structure. All studies reported in the literature have dealt mainly with the resistivity and transmission of Sb:SnO_2 films [10–15] and less care has been devoted to the study of their other optical and electrical parameters.

Homogeneity of thin Sb:SnO_2 film elaborated by usual thermal evaporation from its bulky form prepared by usual melt quench technique may be difficult to achieve due to large differences in thermal parameters (such as melting and boiling points) of SnO_2 and Sb. This leads, in most cases, to form bulk alloy, which consists of separated Sb and SnO_2 phases. These separated materials have very different vapour pressures at the evaporation temperatures and consequently they would evaporate at very different rates to give films with compositions different from that of the source material. For this reason and others concerning with technical applications and economic usefulness, many techniques such as reactive sputtering [16,17], reactive evaporation [18], chemical vapour deposition [19] and pyrolysis of stannic compounds [20] have been employed to deposit thin SnO_2-based films on several substrates. To our knowledge, there is no data available in the literature on Sb–Sn–O films prepared by electron beam evaporation. In the present study, we have used electron beam evaporation to prepare thin Sb–Sn–O films from bulk tablets prepared by sintering after mixing and pressing the appropriate amounts of SnO_2 and Sb powders. Sintering process is an inexpensive method for producing lumps of powdered materials in a bulky form without affecting their chemical properties, while their physical properties approach those of single crystal phase [21]. Besides, the high degree of control possible with electron beam sources, which provide economical and efficient usage of evaporant, enables constant rate deposition.

The aim of the present work is to investigate the effect of antimony doping on the optical and electrical properties of the electron beam evaporated Sb–Sn–O films from their bulky form prepared by sintering technique. The thickness of the used films was about 100 nm, which is the employed

* Corresponding author.

0022-3697/00/$ - see front matter © 1999 Elsevier Science Ltd. All rights reserved.
PII: S0022-3697(99)00234-6

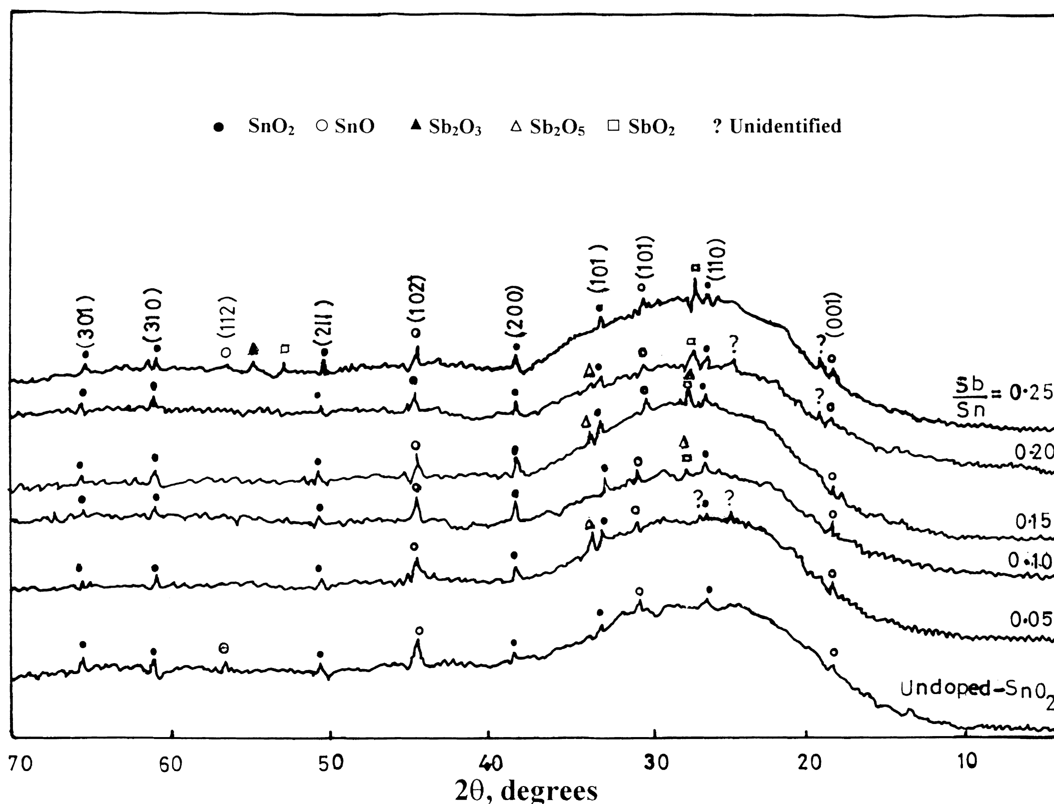

Fig. 1. X-ray diffraction patterns for undoped and Sb-doped SnO_2 thin films.

thickness for many applications [22–24]. A study of the change in some optical and electrical parameters with Sb content has been also considered.

2. Experimental details

Portions of powdered highly pure SnO_2 and Sb were ground separately by means of an agate mortar and pestle. Appropriate ratios of Sb and SnO_2 that passed through a sieve piece of 100 μm mesh but which were retained by one of 54 μm mesh were thoroughly mixed and prepared in a tablet form using cold pressing technique. The contents of Sb (in atomic weight) were taken in the ratio Sb/Sn = 0, 0.05, 0.10, 0.15, 0.20 and 0.25. In order to increase the diffusion process and consequently improve the homogeneity of the material, the tablets were heated at ~600°C for 5 h. Sintering (which is often associated with the formation of new bonds, densification and may be grain growth [21]) of these tablets was carried out at 900°C for 4 h in air.

The present films were deposited onto ultrasonically cleaned corning glass substrates by electron beam evaporation at 2×10^{-5} Torr using an Edwards high vacuum coating unit model E306A. Substrates were heated at 300°C during film deposition using a resistance heater and a chromel–alumel thermocouple monitored their temperatures. The rate of deposition and the thickness of the films were controlled to be about 10 nm min^{-1} and 90–100 nm, respectively, by means of a digital film thickness monitor model TM200 Maxtek. Silver paste electrodes with electrode separation of 2 mm were used.

Investigations of the microstructure were carried out using an X-ray diffractometer (Philips model PW1710) and scanning electron microscope (Joel JSM-5300). A Jasco V-570 UV–visible–NIR spectrophotometer (with photometric accuracy of ± 0.002–0.004 absorbance and ± 0.3% transmittance) was employed to record the transmission and reflection spectra over the wavelength range 200–2500 nm at normal incidence. Optical parameters namely absorption coefficient α_0, refractive index (n), extinction coefficient (K), dielectric constant ϵ', were calculated as described elsewhere [25].

By means of a variable temperature liquid nitrogen cryostat (Oxford DN-1710) combined with programmable temperature controller (Oxford ITC4) and a digital (Keithly 614) electrometer the film resistivity was measured in the temperature range 80–475 K.

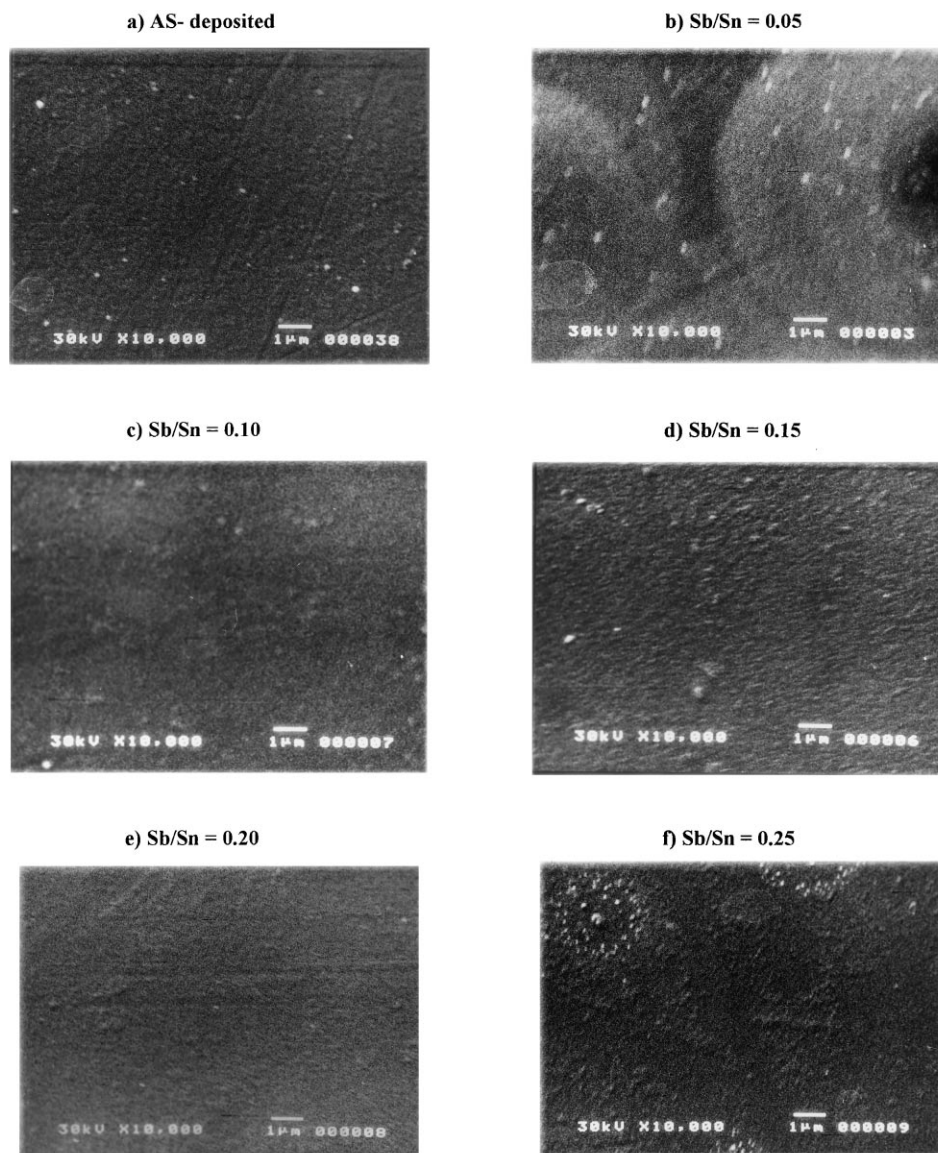

Fig. 2. SEM topographs of Sb–Sn–O films with different Sb-contents.

3. Results

The X-ray diffraction patterns for undoped and Sb-doped SnO_2 films are as shown in Fig. 1. It is clear that all films seem to be partially amorphous. Small peaks corresponding to SnO_2 and SnO crystalline phases, which are embedded in the amorphous matrix, could be observed for the undoped film and is slightly affected in intensity with the increase of Sb-doping. Addition of Sb inside the SnO_2 film leads to the appearance of two non-intensive unidentified phases and one other corresponding to the Sb_2O_5 oxide. A diffraction peak characterizing SbO_2 oxide appears and seems to increase in intensity with further increase in Sb content. Besides, it is observed that, for heavily Sb-doped SnO_2, peaks characterizing the SnO_2 phase shift to lower values of 2θ indicating the increase of lattice constant [10]. This suggests that some of the Sn^{4+} ions in the SnO_2 lattice are replaced by Sb^{3+} ions having larger ionic radius [26,27].

Fig. 2 shows the scanning electron microscope (SEM) topographs of undoped and Sb-doped SnO_2 films. It is evident that the surface of undoped film seems to be smooth and contains few small grains confirming the nearly amorphous nature of the film. For the film having Sb/Sn = 0.05, more grains could be observed in the amorphous matrix and may be attributed to the new phases formed due to the Sb addition. With further increase of Sb content, the surface

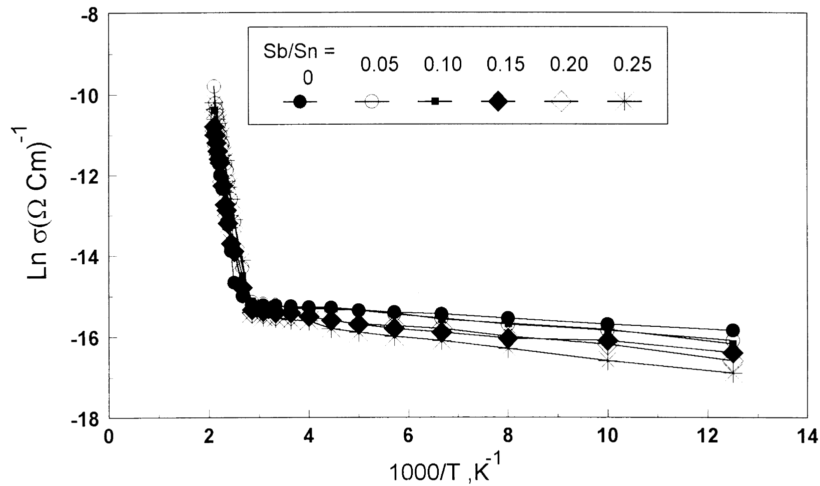

Fig. 3. ln σ versus $1/T$ plots for undoped and Sb-doped SnO_2 films.

tends to be more smooth indicating the increase of film amorphinity with Sb-doping. Aggregation of grains observed for the heaviest Sb-doped films, might be related to the grown, especially SbO_2, phases identified by X-ray diffractograms shown in Fig. 1.

Fig. 3 shows the temperature dependence of the electrical conductivity $\sigma(T)$ plotted in the form of ln σ versus $1/T$ for films having Sb/Sn = 0, 0.10, 0.15, 0.20 and 0.25 in the temperature range from 80 to 475 K. Two distinct regions of $\sigma(T)$ corresponding to the low and high temperature ranges are observed. In the high temperature region (375–475 K) the abrupt increase in σ means that the conduction is thermally activated and assumed to arise from the contribution of the conduction between the extended states. This behaviour of $\sigma(T)$ is well described by the simple Arrhenius law, $\sigma(T) = \sigma_0 \exp(-\Delta E/\mathrm{K}T)$, where ΔE is the corresponding activation energy and σ_0 the pre-exponential factor. The calculated values of both ΔE and σ_0 are given in Table 1. It is seen that uncertainties in the values of both parameters are excessively high. Similar high uncertainties in some electrical and optical parameters such as Hall mobility, number of carriers and band gap have been found by Terrier et al. [14] for $Sb:SnO_2$ films elaborated by the sol–gel method. However, a tendency for a decrease in both ΔE and σ_0 values with Sb incorporation may be noticed here. This may confirm the correlation of the change in ΔE, which is a function of the electronic energy levels of the chemically interacting atoms in the glass, with the corresponding change in σ_0, which includes the carrier mobility and density of states.

In the wide low temperature region (80–375 K), $\sigma(T)$ exhibits relatively less thermal activation, which is characterized by hopping conduction between the localized states. As shown in Fig. 4, the conductivity data in this low temperature region, which are replotted as $\ln \sigma\sqrt{T}$ versus $(1/T)^{1/4}$ and well fitted by straight lines, satisfy Mott's formula for variable-range hopping [28] $\sigma(T) = \sigma_0'/\sqrt{T} \exp[-(T_0/T)^{1/4}]$, where $T_0 = 16\alpha^3/\mathrm{K}N(E_f)$, σ_0' is the pre-exponential factor, $N(E_f)$ is the density of localized states at the Fermi level, α describes the spatial extent of the localized wave function and is assumed to be 0.124 $\mathrm{\AA}^{-1}$ [29] and K the Boltzmann constant. Values of σ_0', T_0, $N(E_f)$, as well as the room temperature values of the hopping distance R and hopping energy W (in Mott's theory $R = [9/8\pi\alpha \mathrm{K}TN(E_f)]^{1/4}$ and $W = 3/4\pi R^3 N(E_f)$) were calculated and are listed in Table 1. From this table, it is observed that the necessary conditions for Mott's variable-range hopping process $W > \mathrm{K}T$ and $\alpha R \gg 1$ are, in

Table 1
Variations of the electrical activation energy ΔE, the pre-exponential factor σ_0 and Mott's parameters T_0, σ_0', $N(E_f)$, and room temperature values of R and W with Sb/Sn ratio

Sb/Sn	ΔE (eV)	$10^{-2}\sigma_0$ (Ω^{-1} cm^{-1})	$10^{-5}T_0$ (K)	$10^{-3}\sigma'_0$ (Ω^{-1} cm^{-1} K$^{1/2}$)	$10^{-21}N(E_f)$ (eV^{-1} cm^{-3})	10^7R (cm)	W (meV)
0	0.44–0.92	1.92–3.72	0.17–0.45	0.35–0.61	4.13–10.92	1.06–1.35	12.5–33.05
0.05	0.48–0.86	4.54–7.54	0.16–0.70	4.37–10.17	2.65–11.61	1.04–1.51	9.93–43.49
0.10	0.35–0.97	1.90–3.60	0.33–1.11	2.59–6.27	1.67–5.63	1.25–1.70	13.22–44.57
0.15	0.42–0.88	0.92–1.80	0.46–1.38	2.55–6.25	1.35–4.04	1.36–1.79	15.13–45.28
0.20	0.44–0.82	0.74–1.38	0.45–1.61	2.00–5.80	1.15–4.13	1.86–1.35	13.99–50.23
0.25	0.34–0.88	0.75–1.33	0.90–3.34	0.98–2.74	0.56–2.06	1.61–2.23	16.38–60.26

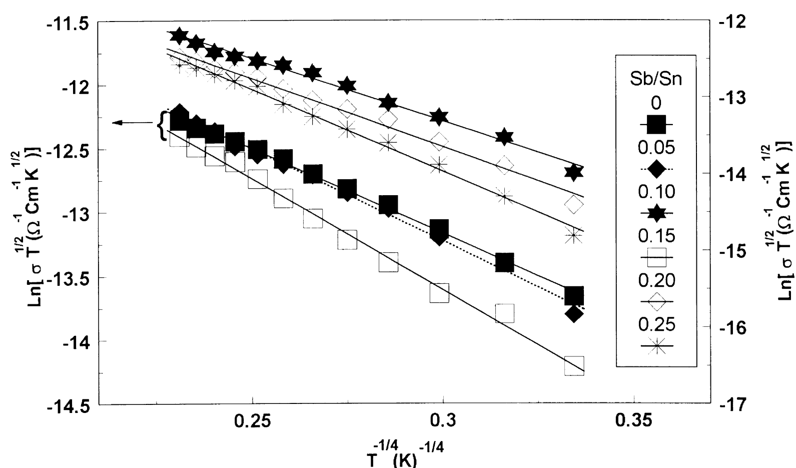

Fig. 4. Plots of ln $\sigma T^{1/2}$ versus $(1/T)^{1/4}$ for undoped and Sb-doped SnO_2 films.

general, satisfied. On the other hand, the increase observed, in general, in R and W values gives an impression that the initial and final states of hopping below and over Fermi level, respectively, may be displaced far from the Fermi level, a matter that could be explained regarding the observed decrease in $N(E_f)$ shown in Table 1.

In order to illustrate the effect of Sb-doping on the film resistivity (ρ) measured at room temperature, the relation of ln ρ versus Sb/Sn ratio is represented in Fig. 5. The resistivity of the undoped film is 4.14×10^6 Ω cm. With addition of Sb the resistivity slightly decreases to a value of 3.86×10^6 Ω cm at Sb/Sn = 0.05 and then it increases with further addition of Sb reaching the value 5.64×10^6 Ω cm at Sb/Sn = 0.25. Thus, all films seem to be very resistive and the resistivity variation with Sb-doping is small compared with the results reported before [3,7,8] for films elaborated by other techniques.

Fig. 6 shows the variations of transmittance (T), reflection (R) and absorption coefficient (α_0) in the wavelength range from 200 to 2500 nm for undoped and Sb-doped SnO_2. It is observed that all films have absorption edge at a wavelength of around 300 nm. Maximum transmittance of undoped film is clearly seen at 750 nm. With increasing Sb-doping this maximum of transmission shifts towards lower values of wavelength (λ) to be at about 500 nm, which is the solar maximum wavelength, for heavily Sb-doped films. These maximum values are about 70, 71.2, 80.4, 81.1, 78.5 and 77.2% for films with Sb/Sn = 0, 0.05, 0.10, 0.15, 0.20 and 0.25, respectively. In the NIR spectral region while the reflection and absorption decrease, the transmission increases with increasing λ, confirming the high transparency of the present films in the NIR as well as the visible spectral regions. At constant value of wavelength ($\lambda = 500$ nm) while T increases, both R and α_0 decrease with increasing Sb/Sn. Besides, as seen from Table 2, the average value of T in the visible (270–780 nm) spectral region increases from about 21 to 62% with increasing the ratio Sb/Sn from 0 to 0.25. This means that the increase of

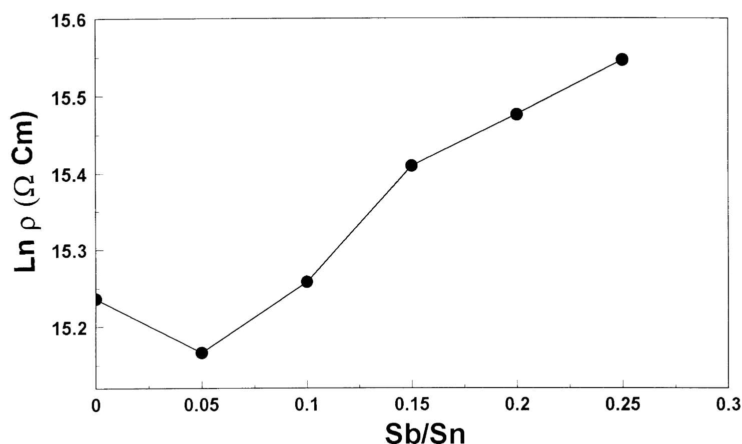

Fig. 5. Variation of ln ρ with Sb/Sn ratio.

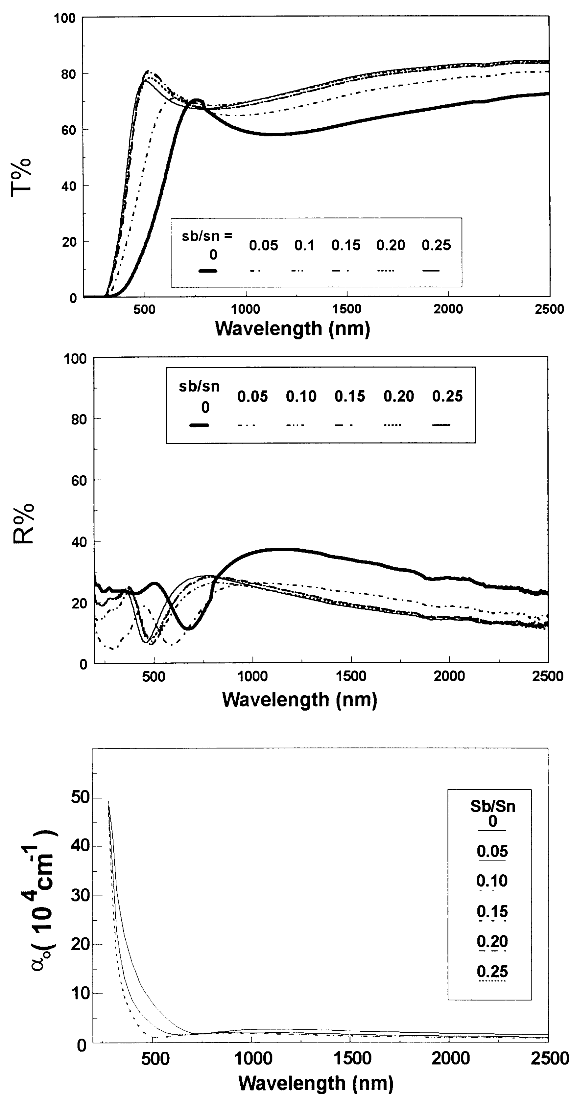

Fig. 6. Transmittance (T%), reflection (R%) and absorption coefficient (α_0) of undoped and Sb-doped SnO_2 films in the wavelength range from 200 to 2500 nm.

Sb content in SnO_2 films improves their transparency in this spectral region.

Sb-doping effects on the refractive index (n) and the extinction coefficient (K) may be clear from the results listed in Table 2. It is seen that n decreases with increasing Sb/Sn from 0 to 0.05 and then increases for heavier Sb-doping. However, K decreases with Sb-content for all Sb-doped films as a consequence of the decrease in α_0 with the latter.

Spitzer and Fan [30] have shown that the contribution from the free carrier electric susceptibility to the real dielectric constant ϵ' can be written as: $\epsilon' = \epsilon_i - e^2/\pi c^2(N/m^*)\lambda^2 = n^2 - k^2$ and $e^2/\pi c^2(N/m^*)\lambda^2 = -4\pi\chi_c$, where ϵ_i is the infinitely high frequency dielectric constant (or lattice dielectric constant), N/m^* is the ratio of carrier concentration to the effective mass and χ_c is the electric free carrier susceptibility. Good fitting to straight lines for the relations ϵ' versus λ^2 and $\ln(-4\pi\chi_c)$ versus $\ln\lambda$ in the NIR (from 2100 to 2500) region are seen in Figs. 7 and 8, respectively. Values of ϵ_i, N/m^* and the average value of χ_c were estimated from these plots and recorded as functions of the ratio Sb/Sn in Table 2. It is observed that all parameters ϵ_i, N/m^* and $|\chi_c|$, in general, seem to decrease with increasing Sb/Sn ratio.

In agreement with the results reported by Kojima et al. [12] and Jousse [31], the intercepts of linear portions of the $(\alpha_0 h\nu)^{1/2}$ versus $h\nu$ plots near the absorption edge to $(\alpha_0 h\nu)^{1/2} = 0$ have been employed to deduce the width of the optical band gap E_g as shown in Fig. 9. The estimated values of E_g are given in Table 2 as a function of the Sb/Sn ratio. Besides, as seen from Fig. 9, exponential tails characterizing amorphous materials appear in the plots. Tauc [32] believes that such exponential variation of α_0 with $h\nu$ is due to transitions between localized states and will vary from sample to sample.

4. Discussion

Results of the resistivities (ρ) measured at room temperature as a function of Sb/Sn ratio shown in Fig. 5, indicate that, although the variation of $\ln\rho$ versus Sb/Sn is different in behaviour with some reported results of Sb–Sn–O films elaborated by other techniques (for example Ref. [14]), it is somewhat similar to that obtained by Kojima et al. [10] and

Table 2
Variations of the optical gap E_g and the average values of n, K and T in the visible spectral region and values of ϵ_i, N/m^* and $-\chi_c$ in the NIR region with the Sb/Sn ratio

Sb/Sn	E_g (eV)	n	K	T	ϵ_i	N/m^* (10^{20} cm^{-3})	$-\chi_c$
0	1.64–2.28	2.56	0.310	0.21	10.85–14.35	7.80–9.92	0.30–0.38
0.05	2.08–2.56	2.08	0.179	0.31	6.58–8.22	3.9–4.76	0.15–0.19
0.10	2.23–2.67	2.49	0.125	0.43	5.01–6.19	2.27–2.73	0.09–0.11
0.15	2.24–2.76	2.62	0.124	0.45	5.29–6.51	2.72–3.28	0.11–0.13
0.20	2.28–2.76	2.63	0.122	0.51	5.30–6.50	2.74–3.26	0.11–0.13
0.25	2.32–2.80	2.68	0.123	0.62	4.88–5.92	1.84–2.16	0.09–0.11

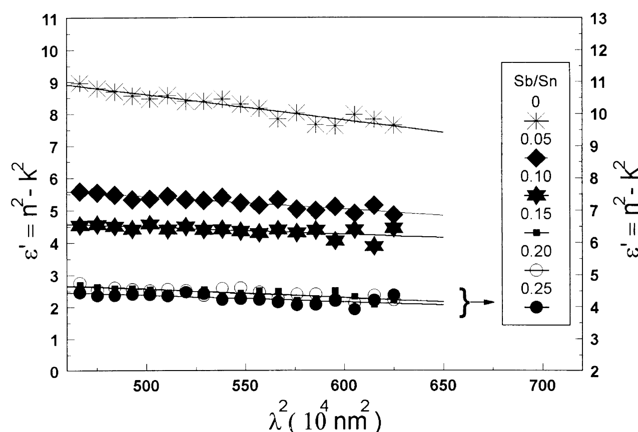

Fig. 7. Plots of the optical dielectric constant ϵ' of undoped and Sb-doped SnO_2 films versus λ^2.

Tsunashima [33] for films prepared by spray pyrolysis at a temperature of 500°C and thermal decomposition of tin 2-ethyl hexanoate and antimony tributoxide at 600°C, respectively. However, the present films are more resistive, a matter that can be attributed to their relatively smaller thickness and higher degree of amorphization. The relatively low resistivity observed for the undoped film is attributed to the deviation from stoichiometry due to oxygen vacancies [26,27], which act as electron donors and increase the free carrier concentration [34]. The slight decrease in resistivity of the film with $Sb/Sn = 0.05$ could be attributed to the small excess of free electrons produced when some of the Sb^{5+} ions are substituted on the Sn^{4+} sites, where the antimony acts as an effective donor. Besides, the increase of resistivity for films with $Sb/Sn \geq 0.10$ may be resulted from the increase of amorphization in films due to Sb-doping [26] rather than the compensation process, which can occur between the two n- and p-types of conduction [10,33,35,36]. Regarding the X-ray diffractograms in Fig. 1, it can be concluded that the trivalent Sb^{3+} component appears and its concentration is increasingly important for heavily Sb-doping which acts as an acceptor. Then, the electrons created by the oxygen vacancies or Sb^{5+} may be trapped by the acceptor levels and the SnO_2 becomes compensated. Thus, the observed increase in the resistivity with increasing Sb-doping can be predicted.

It is observed from Table 1 that the density of states $N(E_f)$ possesses relatively high values. Similar results for amorphous thin films have been reported [37] and attributed to the uncertainties involved in estimating the parameters T_0 and σ'_0 since, a large number of simplifying assumptions are introduced on Mott's relation. However, we think that the present high values of $N(E_f)$ may be reasonable regarding the additional states at E_f owing to the creation of SnO on the expense of SnO_2, which increases the disorder in the SnO_2 film [41]. Besides, the conclusion that the addition of Sb impurities inside the SnO_2 films lead to a decrease of the localized density of states $N(E_f)$ participating in the hopping conduction, which is proved experimentally here as shown in Table 1, have been emphasized by Kojima et al. [10].

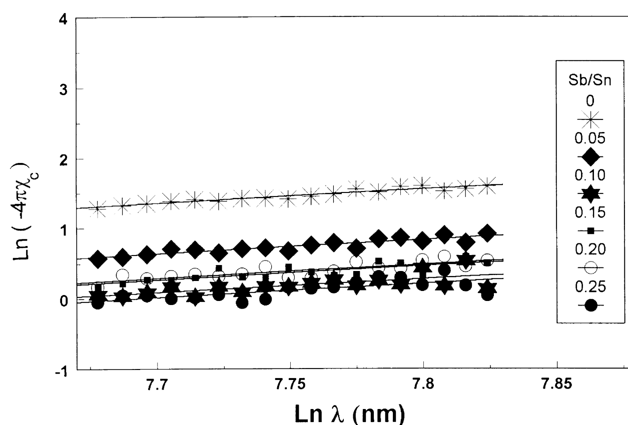

Fig. 8. Plots of $\ln(-4\pi\chi_c)$ of undoped and Sb-doped SnO_2 films versus $\ln\lambda$.

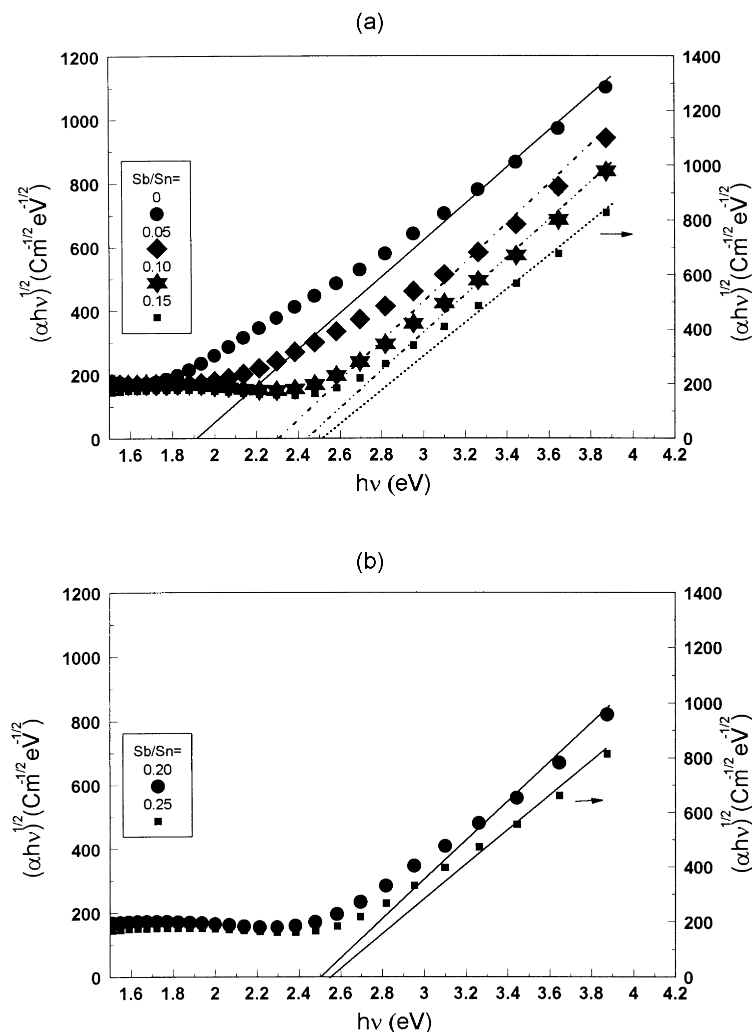

Fig. 9. $(\alpha h\nu)^{1/2}$ against $h\nu$ plots for undoped and Sb-doped SnO_2 films.

They have observed that as [Sb]/[Sn] increases from 0.04 up to 0.23 the density of states decreases from 8×10^{19} to 2×10^{19} eV^{-1} cm^{-3} for SnO_2 films elaborated by spray pyrolysis. As shown in Fig. 10, these results may be explained on the basis of the increase in the energy of the bonds joining together the atoms in the films owing to Sb-doping [10]. In fact, the energy of the states introduced by the Sb–O bonds is larger than that of Sn–O [38] and, therefore, they lie at energy levels which are outside the band region of the SnO_2. This may indicate that the Fermi level E_f lies more deeply within the band gap and consequently, the Sb that acts as the glass former [26] does not participate in the creation of carriers. This may be supported regarding the decrease in the ratio of carrier concentration to the effective mass (N/m^*) with increasing Sb content as shown in Table 2. This means that, as E_f moves farther away from the conduction band mobility edge due to the increase in Sb content, the number $N(E_f)$ of localized states participating in the hopping conduction is expected to decrease.

From the transmission data shown in Fig. 6 and the change in average T with Sb-content in the visible spectral region listed in Table 2, it is proved that the present partially amorphous films are transparent and the average T increases with increasing Sb-doping. The reasons why the crystalline Sb–Sn–O thin films are black whereas the amorphous films are colourless have been discussed in detail by Kojima et al. [12,13]. They have reported that the blackening of the polycrystalline films results from the interaction between Sb^{3+} and Sb^{5+} ions which are randomly substituted in the SnO_2 (rutile type structure) lattice. In this process which is known as quantum-mechanical resonance, the electron exchange among ions which differ in valency gives rise to abnormally deep and intense coloration [39]. Such a process can be observed also in the compounds containing ions of the

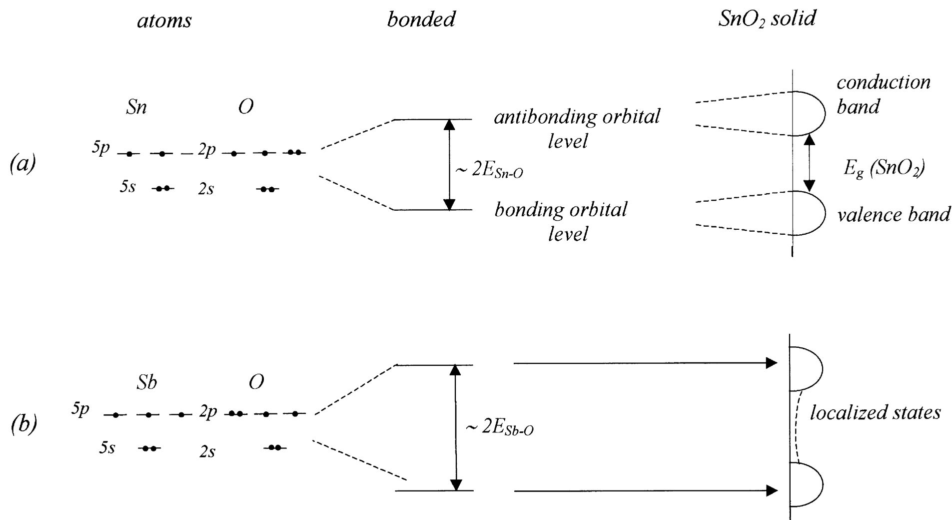

Fig. 10. Energy diagram of the bonding in the case of (a) SnO_2 and (b) with Sb-incorporation in the amorphous film. Localized states, which exist in the band gap, may be originated from the dangling and/or distorted bonds. The bonding energy E_{Sb-O} of the Sb–O bond is larger than E_{Sn-O} corresponding to the Sn–O bond, so the bonding and antibonding levels of Sb–O bond lie outside the band gap of SnO_2.

same element in two different states of oxidation. These compounds (such as SbO_2, which consists of Sb^{3+} and Sb^{5+} instead of Sb^{4+} ions) are termed mixed-valence compounds [40]. These two states of oxidation must be symmetric to each other and energetically equivalent. Besides, it is also necessary for Sb^{3+} and Sb^{5+} ions to be in exactly equivalent sites, i.e. every cation must be surrounded by six anions in octahedral coordination. However, in the present amorphous Sb–Sn–O films these conditions are not verified due to the asymmetrical atmosphere around ions owing to the increasing disorder in the amorphous structure. In addition, the deficiency in oxygen content which may be associated with the formation of SnO compound in the SnO_2 films [41], makes the coordination of the Sb^{3+} and Sb^{5+} to be different. These differences in coordinations of the Sb^{3+} and Sb^{5+} ions and the asymmetrical atmosphere around them make it difficult for electron transfer to take place. Consequently, these films seem to be colourless [40]. Thus, the increase of the number of oxygen vacancies and/or the amorphization in Sb–Sn–O films with Sb-doping should lead to the increase of their transparency.

As shown in Table 2, although high uncertainties could be observed in the values of E_g, it seemed to be improved by Sb-doping. Similar increase in E_g of SnO_2 films with Sb-doping has been noticed formerly [12] and attributed to the increase in the atomic bond energy with Sb incorporation. From the other side, the present results of E_g are rather different from those found by Terrier et al. [14]. They could not attribute the difference between Sb-doped SnO_2 ($E_g = 3.85 \pm 0.2$ eV) and undoped SnO_2 ($E_g = 4 \pm 0.2$ eV) to a decrease of the optical gap due to the presence of doping states into the forbidden band since the material was degenerated. Uncertainties were too high to state that there was a modification of the optical gap after doping. Besides, values reported for E_g of Sb-doped and undoped-SnO_2 films by different authors [10,14,42,43], which vary between 3.1 and 4.1 eV, are higher than its present values. This may confirm the high dependence of E_g on the film elaboration method. On the other hand, the relatively small value of E_g of the present film may be caused by the high degree of disorder in the film. In addition, the used substrate temperature (300°C) during film deposition was too low to improve its crystallinity. Moreover, as seen from Tables 1 and 2, the values of the optical band gap E_g is about two to four times larger than those corresponding to the high temperature activation energy ΔE. This has been observed for some oxides and chalcogenide glasses (see for example Ref. [44]) and attributed to that the electronic activation is not across the whole mobility gap but is possibly from one or more trapping levels to the conduction band or from bonding states to a trapping level.

Besides, several possible reasons that can contribute to the increase in the refractive index (n) have been proposed [45]. The observed abrupt decrease in (n) for the present film having Sb/Sn = 0.05 as shown in Table 2, may be due to the decrease in material compactness as a consequence of the glass network formation by Sb atoms. With further increase in Sb content the reflection decreases as seen from Fig. 6, due to the decrease in carrier concentration, which lead to the observed increase in the refractive index for films with higher Sb-doping. Finally, as shown in Table 2, both the lattice dielectric constant ϵ_i and the electric free carrier susceptibility $|\chi_c|$, in general, decrease with increasing Sb-doping. The decrease in ϵ_i may be attributed to the increase in the concentration of impurity Sb atoms inside SnO_2 films, which results in an increase of the disorder in the structure

matrix [26]. Besides, the decrease of electric susceptibility could be correlated to the decrease observed in free carrier concentration as Sb-content increases.

5. Conclusions

The high resistivity of undoped and Sb-doped SnO_2 films may be mainly attributed to the high degree of amorphization in their structures. This resistivity seemed to be dependent on the content of Sb, which may replace as pentavalent Sb^{5+} and/or trivalent Sb^{3+} ions in Sn^{4+} sites and acts as donor and/or acceptor impurities, respectively. The maximum values of the transmission of films lie at solar maximum and exceed 80% for some cases, which can be considered as a good result. Besides, the average transmission value of films in the visible range has been found to increase with Sb content and interpreted in terms of the interaction between antimony in the two different oxidation states in the SnO_2 lattice. Addition of Sb to SnO_2 films, which forms a glass network in the structure and makes the Fermi level to be shifted farther away from the conduction band, has proved to have significant effects on all other considered electrical and optical parameters.

Accordingly [12,13], it may be concluded that amorphous Sb–Sn–O films are transparent and the enhancement of their electrical properties may depend on the formation of Sb–O oxides. As it is proved in Fig. 1, the main feature of the elaborated films from the initial bulk $Sb{:}SnO_2$ material prepared using sintering technique may be the creation of the Sb–O bonds. This confirms that the bulk Sb–Sn–O material prepared by the sintering method is still promising initial material for producing transparent conductive films. Performing the sintering for longer time and higher temperature for the initial bulk material and annealing the elaborated films at suitable conditions may improve simultaneously the electrical and optical properties of the present films, which is the project of our future work.

Acknowledgements

The authors would like to thank Dr Masahiko Kojima (Nagoya Municipal Industrial Research Institute, Japan) for his useful help in discussion and providing the energy diagram of the present material. Thanks are also due to Prof M.M. Ibrahim (University of South Valley, Egypt) for his useful comments and sincere encouragement in this study.

References

[1] A. Messad, J. Bruneaux, H. Cachet, M. Froment, J. Mater. Sci. 29 (1994) 5095.
[2] R. Bellingham, W.A. Phillips, C.J. Adkins, J. Mater. Sci. 11 (1992) 263.
[3] R.N. Ghosthagore, J. Electrochem. Soc. 125 (1978) 110.
[4] T. Maruyama, K. Tabata, J. Appl. Phys. 68 (1990) 4282.
[5] A. Smith, J.M. Laurent, D.S. Smith, J.P. Bonnent, R. Rodriguez-Clemente, Thin Solid Films 266 (1995) 20.
[6] G. Gordillo, L.C. Moreno, W. de la Cruz, P. Teheran, Thin Solid Films 252 (1994) 61.
[7] J.C. Manifacier, L. Dzepessy, J.F. Bresse, M. Perotin, Mater. Res. Bull. 14 (1979) 163.
[8] W. Spence, J. Appl. Phys. 38 (1967) 3767.
[9] Tar-Sun Hsu, S.K. Ghandi, J. Electrochem. Soc., Solid State Sci. Technol. 127 (1980) 1592.
[10] M. Kojima, H. Kato, M. Gatto, Phil. Mag. B 68 (2) (1993) 215.
[11] M. Kojima, H. Kato, M. Gatto, Phil. Mag. B 73 (1996) 289.
[12] M. Kojima, H. Kato, M. Gatto, Phil. Mag. B 73 (1996) 277.
[13] M. Kojima, H. Kato, M. Gatto, J. Non-Cryst. Solids 218 (1997) 230.
[14] C. Terrier, J.P. Chatelon, J.A. Roger, Thin Solid Films 295 (1997) 95.
[15] M. Yamanaka, Y. Hayashi, Solar Energy Mater. 17 (1988) 407.
[16] B. Stjenna, C.G. Granqvist, Solar Energy Mater. 20 (1990) 225.
[17] E. Leja, T. Pizarkiewicz, A. Kolodziej, Thin Solid Films 67 (1980) 45.
[18] H. Demiryont, N. Tezey, Thin Solid Films 101 (1983) 345.
[19] A.K. Saxena, R. Thangaraj, S.P. Single, P. Agnihorti, Thin Solid Films 131 (1985) 121.
[20] M.B. Gottlieb, R. Koropecki, R. Arce, R. Crisalle, J. Ferron, Thin Solid Films 199 (1991) 13.
[21] W.D. Kingery, in: W. Kingery (Ed.), Kinetics of High Temperature Processes, MIT Press, Cambridge, MA, 1959, pp. 187.
[22] F. Decker, J. Melsheimer, H. Gerischer, Isr. J. Chem. 22 (1982) 195.
[23] W. Badawy, F. Decker, K. Doblhofer, Solar Energy Mater. 8 (1983) 363.
[24] W. Badawy, K. Doblhofer, I. Eiselt, H. Gerischer, S. Krause, J. Melsheimer, Electrochem. Acta 29 (1984) 1617.
[25] E.Kh. Shokr, J. Phys. Chem. Solids 53 (1992) 1215.
[26] A.F. Carroll, L.H. Slack, J. Electrochem. Soc. 123 (1976) 1889.
[27] I.S. Mulla, A.S. Soni, V.J. Rao, A.P. Sinha, J. Mater. Sci. 21 (1986) 1280.
[28] N.F. Mott, E.A. Davis, Electronic Processes in Non-Crystalline Solids, Clarendon Press, Oxford, 1979.
[29] H. Fritsche, in: J. Tauc (Ed.), Amorphous and Liquid Semiconductors, Plenum, London, 1974, pp. 221.
[30] W.G. Spitzer, H.Y. Fan, Phys. Rev. 106 (1957) 882.
[31] D. Jousse, Phys. Reo. 31 (1985) 5335.
[32] J. Tauc, in: F. Abele's (Ed.), Optical Properties of Solid, Elsevier, Amsterdam, 1971, pp. 277.
[33] A. Tsunashima, H. Yoshimiza, K. Kodaira, S. Shimada, T. Matsushita, J. Mater. Sci. 21 (1986) 2731.
[34] J.C. Fan, B. Goodenough, J. Appl. Phys. 48 (1977) 3524.
[35] K.H. Kim, S.W. Lee, D.W. Shin, G.G. Park, J. Am. Ceram. Soc. 77 (1994) 915.
[36] E. Shanti, V. Dutta, A. Banerjee, K.L. Chopra, J. Appl. Phys. 51 (1980) 6243.
[37] R.M. Mehra, R. Kumar, P.C. Mathur, Thin Solid Films 170 (1989) 15.
[38] W.D. Kingery, H.K. Bowen, D.R. Uhlmann, Introduction to Ceramics, Wiley, New York, 1976, p. 99.

[39] K. Nassau, Am. Mineral 63 (1978) 219.
[40] M.B. Robin, P. Day, Adv. Inorg. Chem. Radiochem. 10 (1967) 247.
[41] G.A. Khan, C.A. Hogarth, J. Mater. Sci. 25 (1990) 3002.
[42] J. Robertson, J. Phys. C 12 (1979) 4767.
[43] T.J. Godin, J.P. Lafemina, Phys. Rev. B 47 (1993) 6518.
[44] M.A. Hassan, C.A. Hogarth, J. Mater. Sci. 23 (1988) 2500.
[45] E. Bertran, A. Lousa, M. Varela, M.V. Cuenca, J.L. Morenza, Solar Energy Mater. 17 (1988) 7890.